Research Square

Preprints are preliminary reports that have not undergone peer review.
They should not be considered conclusive, used to inform clinical practice,
or referenced by the media as validated information.

Modeling multicomponent metal-ion transport in an electrodeionization cell for the treatment of lithium-ion battery leachates

Isidro Juvenal González-Panzo

isjuv.gp@gmail.com

Tecnológico Nacional de México/Tecnológico de Estudios Superiores de Ecatepec

Rosa Angelica Bustamante-Rendon

Tecnológico Nacional de México/Tecnológico de Estudios Superiores de Ecatepec

Francisco Javier Almazán-Ruiz

Universidad Nacional Autónoma de México

Gustavo Aparicio-Mauricio

Tecnológico Nacional de México/Tecnológico de Estudios Superiores de Ecatepec

María Aurora Martínez-Trujillo

Tecnológico Nacional de México/Tecnológico de Estudios Superiores de Ecatepec

Martín R. Cruz-Díaz

Universidad Nacional Autónoma de México

Research Article

Keywords: Electrodeionization, lithium-ion battery recycling, multicomponent ion transport, Nernst–Planck model, ion-exchange membranes, metal-ion separation, current–voltage response, sulfate solutions

Posted Date: November 25th, 2026

DOI: https://doi.org/10.21203/rs.3.rs-11758893/v1

License: This work is licensed under a Creative Commons Attribution 4.0 International License.
Read Full License

Additional Declarations: No competing interests reported.

Modeling multicomponent metal-ion transport in an electrodeionization cell for the treatment of lithium-ion battery leachates

Isidro J. González-Panzo[1,2*], R.A. Bustamante-Rendon[1], F.J. Almazán-Ruiz[3], Gustavo Aparicio-Mauricio[1], María Aurora Martínez-Trujillo[1] and Martín R. Cruz-Díaz[2]

[1]Tecnológico Nacional de México/Tecnológico de Estudios Superiores de Ecatepec, Av. Tecnológico esq. Av. Carlos Hank González, Col. Valle de Anáhuac, Ecatepec de Morelos 55210, México

[2]Departamento de Ingeniería y Tecnología, Universidad Nacional Autónoma de México, Facultad de Estudios Superiores Cuautitlán, Av. Primero de Mayo, Cuautitlán Izcalli, C.P. 54740, Edo. de México, México.

[3]Departamento de Ingeniería y Tecnología, Facultad de Estudios Superiores Zaragoza, UNAM. Col. Ejército de Oriente. Tel: (55)57736331, CP 09239, Iztapalapa, CDMX, México.

Abstract

The recovery of metals from spent lithium-ion batteries requires separation operations capable of treating the multicomponent aqueous solutions generated during leaching. In this work, a two-dimensional mathematical model of an electrodeionization (EDI) cell is developed to investigate the transport of Li^+, Co^{2+}, Ni^{2+}, and Mn^{2+} in a model sulfate solution. The formulation considers Nernst–Planck transport, convection, ion exchange in the diluate compartment, transport through ion-exchange membranes, water dissociation, and electrochemical reactions at the electrodes. The current–voltage response and the time-dependent concentration profiles in the recirculation tanks are evaluated under different feed concentrations and electrical operating conditions. The simulations predict ohmic, limiting-current, and overlimiting regimes. Increasing the concentration in the diluate compartment from 25 to 100 mol m^{-3} raises the estimated limiting current density from approximately 90 to 415 A m^{-2}. Higher current density and electrolyte concentration also enhance the transport of all metal species toward the concentrate compartment. However, Co^{2+} exhibits the greatest accumulation, followed by Li^+; therefore, conditions that increase the overall transport of metal ions do not, by themselves, demonstrate lithium selectivity. The results identify feed concentration and electrical operating conditions as relevant variables for controlling multicomponent transport and indicate that membrane and resin selectivity must be optimized, and the model experimentally validated, before selective Li^+ recovery can be established.

Keywords: Electrodeionization; lithium-ion battery recycling; multicomponent ion transport; Nernst–Planck model; ion-exchange membranes; metal-ion separation; current–voltage response; sulfate solutions.

*Corresponding author:
Isidro J. González-Panzo, isjuv.gp@gmail.com

I. Introduction

The rapid expansion of electric mobility, portable electronics, and renewable energy storage systems has significantly increased the demand for lithium-ion batteries (LIBs), making the sustainable management of end-of-life batteries a major technological and environmental challenge. Spent LIBs represent a valuable secondary resource because they contain substantial quantities of lithium and other critical metals that can be recovered and reintroduced into battery manufacturing and other industrial applications. Recycling these materials can reduce dependence on primary mineral extraction, mitigate the environmental impacts associated with mining, minimize hazardous waste generation, and promote the transition toward a circular economy [1,2]. Consequently, the development of efficient and selective recovery technologies has become essential for closing the materials loop in energy storage systems.

Current LIB recycling strategies primarily rely on pyrometallurgical and hydrometallurgical processes. Pyrometallurgy involves high-temperature treatment to recover valuable metals, offering operational robustness and the ability to process heterogeneous feedstocks. However, it is associated with high energy consumption, potential greenhouse gas emissions, and lithium losses into slag, which may require additional treatment for subsequent recovery. In contrast, hydrometallurgical processes have gained considerable attention because of their potential for selective metal separation, relatively low operating temperatures, and high recovery efficiencies. These processes typically involve battery discharge, dismantling, mechanical separation, and the production of a concentrated active-material fraction commonly known as black mass. The resulting material is subsequently subjected to leaching using mineral acids, such as sulfuric or hydrochloric acid, often in combination with reducing agents such as hydrogen peroxide. Alternative approaches include organic-acid leaching and biological treatments. Despite their advantages, hydrometallurgical routes generate complex

aqueous streams containing dissolved metals, residual reagents, and other impurities that require further separation, purification, and wastewater management [3–5].

The leaching of spent LIB active materials produces multicomponent solutions containing lithium, cobalt, nickel, and manganese, together with other metallic species depending on the battery chemistry, pretreatment conditions, and leaching procedure [6,7]. The selective recovery of lithium from these solutions remains challenging because lithium coexists with transition-metal ions exhibiting different concentrations, charge densities, transport properties, and chemical affinities. Moreover, the presence of competing ions can affect separation efficiency, reagent consumption, product purity, and the overall environmental performance of the recycling process. Several technologies have been investigated to address these challenges, including chemical precipitation, solvent extraction, ion exchange, selective adsorption, electrodialysis, and other membrane-based separation processes. Their suitability depends on the chemical composition of the leachate, the required recovery and purity levels, process economics, and environmental considerations [8–10].

Conventional hydrometallurgical flowsheets generally separate cobalt, nickel, and manganese from lithium-containing solutions through selective precipitation, solvent extraction, or ion-exchange operations. Lithium is subsequently concentrated and purified before conversion into valuable compounds, particularly lithium carbonate or lithium hydroxide, which may serve as precursors for battery manufacturing. Achieving the required product purity can involve several successive separation and purification stages, increasing process complexity and the consumption of chemicals and water. Additional challenges include the generation of secondary waste streams, the need for regenerating chemical agents, and the management of residual salts. These limitations highlight the need for complementary separation technologies capable of improving lithium recovery while reducing chemical inputs and environmental burdens [11,12].

Electrodeionization (EDI) is a hybrid electrochemical separation technology that combines ion-exchange membranes, ion-exchange resins, and an applied electric field to facilitate the continuous removal and transport of ionic species. Although EDI has traditionally been used for ultrapure water production, its ability to integrate membrane transport and resin-mediated ion exchange makes it a promising complementary operation for treating metal-bearing

solutions generated during LIB recycling. Under an applied electric field, dissolved ions migrate through the solution and ion-exchange phases and are transported across selectively permeable membranes, enabling their redistribution between diluate and concentrate streams. Unlike conventional ion-exchange processes that require periodic chemical regeneration, EDI can sustain ion-exchange activity through electrically driven transport and water dissociation under appropriate operating conditions. This characteristic offers the potential to reduce regenerant consumption, facilitate continuous operation, and integrate electrochemical separation into more sustainable hydrometallurgical flowsheets [13,14].

The implementation of EDI in LIB recycling requires, however, careful consideration of feed composition, membrane properties, resin characteristics, operating voltage, current density, and competing transport mechanisms. In particular, the simultaneous presence of monovalent lithium ions and divalent transition-metal ions complicates the prediction of separation performance. Selectivity cannot be attributed exclusively to ionic charge or mobility because it also depends on membrane permselectivity, resin affinity, concentration gradients, solution speciation, and operating conditions. Furthermore, high ionic concentrations, residual impurities, and changes in local solution composition may influence electrical resistance, concentration polarization, water dissociation, and the onset of limiting-current conditions. Therefore, EDI should be considered within an integrated process scheme in which upstream operations control the composition of the leachate and downstream operations recover or convert the concentrated metal streams into suitable products.

Several integration strategies can be considered to exploit the advantages of EDI in battery recycling. Conventional precipitation or solvent extraction may be used upstream to remove substantial fractions of cobalt, nickel, and manganese before the selective treatment of lithium-containing solutions. Alternatively, ion-exchange resins or lithium-selective sorbents may be incorporated into hybrid separation schemes to improve the treatment of dilute streams. Electrodialysis can also provide an initial fractionation step, followed by EDI for further concentration or purification. The selection of an appropriate configuration depends on the desired separation objectives, the initial and final concentrations of the target ions, and the chemical and electrical characteristics of the feed. Process performance should consequently be assessed using complementary indicators, including metal recovery,

separation selectivity, concentration factor, current efficiency, specific energy consumption, product purity, and operational stability [13–15]. These indicators are essential for determining whether EDI can provide a technically viable and environmentally advantageous contribution to integrated LIB recycling.

Despite progress in electrochemical separation technologies, a comprehensive understanding of ion transport in EDI systems treating multicomponent metal-bearing solutions remains necessary. The coupled effects of electromigration, diffusion, convection, membrane transport, and ion exchange determine the distribution of ionic species between the diluate and concentrate compartments. These mechanisms interact with electrode reactions, water dissociation, local variations in pH, and changes in solution conductivity. In multicomponent systems, competition among lithium, cobalt, nickel, and manganese ions introduces additional complexity because the transport rate of each species depends on its concentration, charge, mobility, and interactions with the membrane and resin phases. These coupled phenomena can generate nonlinear current–voltage responses and time-dependent changes in the composition of the treated solutions. Consequently, experimental measurements alone may not provide sufficient information to identify the contribution of individual mechanisms or predict performance beyond the specific conditions investigated.

Mathematical modeling and computational simulation offer a systematic approach to investigate these coupled phenomena and support the design and optimization of EDI systems. A mechanistic model can describe ionic transport and mass conservation while incorporating the electrical response of the cell and the evolution of the concentrations in the diluate and concentrate streams. When appropriately formulated and validated against experimental data, such a model can be used to evaluate the influence of operating variables, identify limiting-current conditions, analyze metal-ion accumulation and depletion, and establish relationships between electrical energy input and separation performance. This approach is particularly relevant to LIB recycling because the composition of real leachates can vary considerably depending on the battery chemistry, pretreatment, and leaching conditions. Predictive simulations can therefore help identify operating windows, assess alternative feed compositions, and reduce the number of experiments required for process development.

In this context, the present study investigates electrodeionization as a selective recovery step within an integrated process for recycling spent lithium-ion batteries, with particular emphasis on mathematical modeling and computational simulation. A multicomponent aqueous solution containing lithium, cobalt, nickel, and manganese sulfates is considered as a representative model feed because these metals are commonly associated with LIB active materials and their hydrometallurgical processing. The modeling framework describes the principal transport and electrochemical phenomena governing EDI operation, including electromigration, diffusion, convection, ion exchange, membrane-mediated transport, water dissociation, and electrode reactions. The model is used to analyze the current–voltage response of the cell, determine the limiting-current behavior, and predict the temporal evolution of metal-ion concentrations in the diluate and concentrate storage tanks.

The influence of applied cell voltage, feed composition, and current density on ionic transport and separation performance is examined through numerical simulations. Particular attention is given to the accumulation of metal ions in the concentrate stream and their depletion from the diluate stream as functions of operating time. These analyses provide insight into the coupled electrical and mass-transfer behavior of the system and establish a basis for evaluating the potential role of EDI in integrated lithium and transition-metal recovery schemes. Rather than assuming intrinsic lithium selectivity, the study examines the transport behavior of the individual metallic species and the extent to which operating conditions influence their separation.

The main contribution of this work is the development and application of a computational framework to analyze EDI operation for multicomponent metal-sulfate solutions relevant to LIB recycling. By linking the current–voltage response with the time-dependent distribution of dissolved metals, the study provides a mechanistic basis for evaluating operating conditions and identifying opportunities for process improvement. The results are intended to support the integration of EDI with upstream leaching and conventional separation operations, as well as downstream metal recovery and product purification. Ultimately, this modeling-based approach may contribute to the development of scalable and resource-efficient recycling flowsheets that improve metal recovery, reduce chemical consumption, and minimize secondary waste generation.

2. Electrodeionization functioning in lithium-ion battery recycling

Electrodeionization (EDI) is an electrically driven separation technology that combines ion-exchange membranes, ion-exchange resins, and a direct-current electric field to selectively transport dissolved ions from a feed solution into concentrated streams. In the context of metal recovery from sulfate leachates generated during the processing of spent lithium-ion batteries (LIBs), EDI represents an advanced purification and concentration technology capable of separating lithium ions from competing transition metals while minimizing the consumption of chemical reagents and reducing secondary waste generation.

As illustrated in Figure 1, the EDI flow cell consists of an anode compartment (AC), a dilute compartment (DC), and a cathode compartment (CC), separated by an anion-exchange membrane (AM) and a cation-exchange membrane (CM). The dilute compartment is filled with a mixed-bed ion-exchange resin that functions as both an ion-conducting medium and a reservoir of ion-exchange sites. The feed solution, containing dissolved sulfate salts of lithium and transition metals such as Co^{2+}, Ni^{2+}, and Mn^{2+}, is continuously introduced into the dilute compartment, where the separation process takes place.

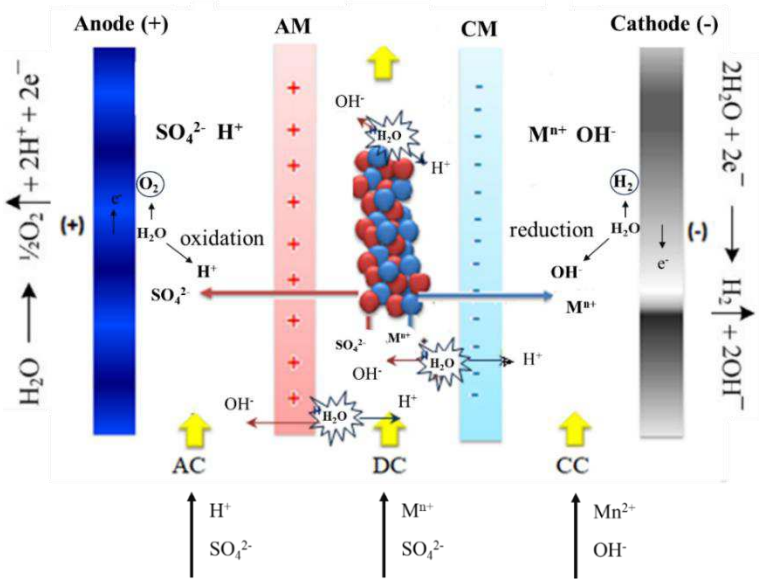


Figure 1. Schematic diagram of the electrodeionization flow cell functioning for metal ion recovery M^{n+} (Li^+, lithium), using a multicomponent metal sulphates solution.

When a direct current is applied between the anode and cathode, an electric potential gradient is established throughout the cell. Under the influence of this electric field, positively charged

ions migrate toward the cathode, whereas negatively charged ions move toward the anode. Consequently, lithium ions (Li^+) and the other metallic cations migrate through the resin bed toward the cation-exchange membrane, while sulfate ions (SO_4^{2-}) move toward the anion-exchange membrane. The cation-exchange membrane selectively permits the transport of cations while rejecting anions, whereas the anion-exchange membrane allows only anion transport and prevents the passage of positively charged species. This selective ion transport continuously removes dissolved ions from the dilute stream and transfers them into adjacent concentrating compartments.

Within the resin-filled dilute compartment, ion transport occurs through a combination of electromigration, diffusion, and ion-exchange mechanisms. Electromigration constitutes the primary transport mechanism, driven by the applied electric field. Simultaneously, concentration gradients generated during operation promote diffusive transport, while ion-exchange reactions occur between dissolved ions and the functional groups attached to the resin matrix. The resin particles temporarily adsorb ions and facilitate their movement through the packed bed, thereby reducing electrical resistance and enhancing overall separation efficiency. Unlike conventional ion-exchange systems, the resin bed in EDI is continuously regenerated during operation by water dissociation phenomenon, eliminating the need for periodic chemical regeneration.

As shown in the figure, sulfate ions migrate across the anion-exchange membrane toward the anode compartment. In the vicinity of the anode, water oxidation occurs according to:

$$H_2O = \frac{1}{2}O_2 + 2H^+ + 2e^- \quad (1.0)$$

This reaction generates protons that contribute to charge balance within the anodic compartment. The accumulation of sulfate ions together with the generated protons maintains electroneutrality and promotes continuous ionic transport from the dilute compartment.

Simultaneously, metallic cations migrate through the cation-exchange membrane toward the cathode compartment. At the cathode surface, water reduction takes place according to:

$$2H_2O + 2e^- = H_2 + 2OH^- \quad (2.0)$$

The formation of hydroxide ions increases the pH within the cathode compartment, while hydrogen gas is released as a byproduct. The transported cations accumulate in the catholyte, producing a concentrated metal-bearing stream. Under controlled operating conditions, lithium can be preferentially enriched in this stream, enabling its subsequent recovery through precipitation, crystallization, solvent extraction, or electrochemical processing.

A distinctive feature of EDI is the occurrence of water dissociation at highly polarized resin–membrane and resin–resin interfaces, as previously said. As ion concentrations decrease within the dilute compartment, the local electric field intensity increases significantly, inducing the dissociation of water molecules according to:

$$H_2O \rightarrow H^+ + OH^- \tag{3.0}$$

The generated H^+ and OH^- ions continuously regenerate the ion-exchange resins in situ. Hydrogen ions migrate toward the cathode side, while hydroxyl ions move toward the anode side, restoring the active ionic forms of the resin functional groups, as shown in Fig. 1. This self-regeneration mechanism maintains the ion-exchange capacity of the resin bed and enables long-term continuous operation without the use of external regenerating chemicals, representing one of the principal advantages of EDI over traditional fixed-bed ion-exchange processes.

For lithium recovery applications, the principal challenge arises from the coexistence of lithium with higher-valence transition-metal ions such as Co^{2+}, Ni^{2+}, and Mn^{2+}. These multivalent ions generally exhibit stronger electrostatic interactions with membrane functional groups and ion-exchange resins than lithium ions. Consequently, lithium selectivity depends on the complex interplay among membrane properties, resin characteristics, feed composition, ionic mobility, hydrated ionic radius, and operating conditions. Parameters such as applied voltage, current density, feed concentration in DC compartment, feed concentration in CC and AC compartments, volume of the reservoir tanks, and resin composition strongly influence ion migration rates and separation performance.

The electric field not only drives ionic transport but also affects the relative migration rates of the different metallic species. Because lithium is a monovalent ion with a relatively high transport mobility, optimized EDI operating conditions can promote its selective migration

while limiting the co-transport of divalent transition metals. The resulting enrichment of lithium in the concentrate stream improves the purity of downstream lithium products and reduces the complexity of subsequent purification stages.

As the process proceeds, ions are continuously removed from the dilute reservoir tank, causing a progressive decrease in total ionic concentration within the feed channel. Simultaneously, transported ions accumulate in the concentrate reservoir tank, producing lithium-rich streams suitable for further processing. The performance of the EDI system is commonly evaluated through lithium removal efficiency, lithium concentration factor, current efficiency, specific energy consumption, and lithium selectivity relative to competing metal ions. Optimization of these performance indicators is essential for maximizing lithium recovery while minimizing energy requirements and undesirable transition-metal transport.

The EDI flow cell operates through the synergistic coupling of ion-exchange, electromigration, membrane selectivity, and water-dissociation phenomenon. The membrane–resin architecture continuously removes ionic species from solution while simultaneously regenerating the ion-exchange medium, enabling sustained operation without chemical regenerants. For the treatment of lithium-bearing sulfate leachates from spent lithium-ion batteries, EDI can provide an effective and sustainable separation technology capable of concentrating lithium and metals, reducing reagent consumption, minimizing waste generation, and enhancing the overall efficiency of battery recycling processes.

3. Mathematical model for the EDI flow cell

In this study, a two-dimensional (2D) mathematical model was developed and proposed to describe ion transport and electrochemical phenomena within an electrodeionization (EDI) cell. The mixed-bed ion-exchange resin contained in the dilute compartment (DC) was represented as a porous medium, enabling the incorporation of ion transport, ion-exchange mass transfer and water dissociation within the resin phase, on the other hand, water electrolysis at the electrode surfaces is also incorporated into a unified modeling framework. The transport of all ionic species was described using the Nernst–Planck equations under a tertiary current distribution formulation coupled with the electroneutrality condition. Ion-exchange between dissolved ions and the charged functional groups of the cationic and anionic resins was represented by an equilibrium adsorption model formulated as a

source/sink term within the porous medium. Water dissociation occurring at the interfaces between oppositely charged resin beads was modeled assuming chemical equilibrium while accounting for the second Wien effect (SWE) induced by the applied electric field. In addition, the electrolysis of water at the cathode and anode was described using kinetic expressions based on the cathodic and anodic Tafel equations evaluated at the water redox equilibrium potential.

3.1 Ions transport model

The transport of ionic species through the EDI cell is modeled using the Nernst–Planck equations, which describe the combined effects of diffusion, electromigration, and convection on ionic fluxes [16]:

$$\boldsymbol{N_i} = -\left(D_i \nabla c_i + z_i u_{m,i} F c_i \nabla \varphi\right) + \boldsymbol{u} \cdot \nabla c_i \tag{4.0}$$

Where, $\boldsymbol{N_i}$ is the vector flux for each ionic species i, whit the migration ($z_i u_{m,i} F c_i \nabla \varphi$), diffusion ($D_i \nabla c_i$), and convection ($\boldsymbol{u} \cdot \nabla c_i$) terms. For each species i, D_i is diffusion coefficient (an effective diffusion coefficient for membrane-resin phase is defined (Eq. 8.0)), c_i is concentration, z_i is the ion charge, $u_{m,i}$ is the ionic mobility ($u_{m,i} = D_i/RT$, Nernst-Einstein relation), R is gas constant, T is absolute temperature, F is Faraday constant, ϕ is the electric potential, $\boldsymbol{u}$ is the velocity vector and the subscript i refers to each transported specie (Li^+, H^+, OH^-, Co^{2+}, Mn^{2+}, Ni^{2+}, SO_4^{2-}). The ions mass transport flux (Nernst-Planck equations, Eq. 4.0) is applied to the entire EDI simulation domain (see Fig. 2): cathodic, anodic and dilute channels, membrane and resins phases (anionic and cationic), and into the cathode and anode surfaces.

The convective term in Eq. (4.0) is evaluated using the electrolyte velocity field obtained from the coupled solution of the Navier–Stokes equations (Eq. (5.0)) and the continuity equation (Eq. (5.1)) [17].

$$(\rho \boldsymbol{u} \cdot \nabla)\boldsymbol{u} = -\nabla P + \nabla \cdot \mu(\nabla \boldsymbol{u} + (\nabla \boldsymbol{u})^T) \tag{5.0}$$

$$\nabla \cdot \boldsymbol{u} = 0 \tag{5.1}$$

Where ρ is liquid density, $\boldsymbol{u}$ is the velocity vector of liquid inside the EDI, P is liquid pressure, μ is liquid viscosity.

The transport of each ionic species i in the EDI channels is governed by the following transient conservation equation [18]:

$$\frac{\partial c_i^l}{\partial t} = -\nabla \cdot \boldsymbol{N}_i^l + R_i = \nabla \cdot \left(D_i^l \nabla c_i^l - \boldsymbol{u} c_i^l + z_i u_{m,i}^l F c_i^l \nabla \varphi^l\right) + R_i \quad (6.0)$$

Where t is time and R_i is a source term. The *"i"* species considered are: Li^+, H^+, OH^-, Co^{2+}, Mn^{2+}, Ni^{2+}, SO_4^{2-}. The "*l*" channels are cathodic (CC), anodic (AC) and dilute (DC).

Electroneutrality condition [19]:

$$\sum z_i c_i^l = 0 \quad (7.0)$$

This constraint enforces the electroneutrality condition within the electrolyte solutions in the EDI channels. In Eq. (7.0), z_i and c_i^l denote the charge number and concentration of ionic species i in channel l, respectively.

The solution of Eqs. (4.0) to (7.0) yields the electric potential and ionic concentration distributions throughout the EDI domain (Fig. 2). These primary variables enable the calculation of derived electrochemical quantities, such as the current density (Eq. (8.0)) and the current continuity equation (Eq. (8.1)) [20]:

$$\boldsymbol{j}^l = F \sum z_i \boldsymbol{N}_i^l = F \sum z_i \left(D_i^l \nabla C_i^l + z_i u_{m,i}^l F C_i^l \nabla \varphi^l\right) \quad (8.0)$$

$$\nabla \cdot \boldsymbol{j}^l = F \sum z_i \boldsymbol{\nabla} \cdot \boldsymbol{N}_i^l + Q_i \quad (8.1)$$

Equation (8.0) describes the current density vector $\boldsymbol{j}^l$, which is derived from the ionic fluxes according to Faraday's law. Under the electroneutrality assumption, the convective contribution vanishes and is therefore omitted from the formulation. Equation (8.1) represents the current continuity equation, where Q_i denotes a volumetric source (or sink) current term with units of A/m^3.

An effective diffusion coefficient $D_{i,eff}$, is employed in Eq. (4.0) to account for the transport of ionic species i within the membrane and resin phases, and is expressed as:

$$D_{i,eff} = \frac{\epsilon_l}{\tau_l} D_i \quad (9.0)$$

Where ϵ_l and τ_l are porosity and tortuosity factors ($\epsilon_l/\tau_l = 0.0315$) [21].

At the interfaces between the cation- and anion-exchange membranes (CM and AM) and the electrolyte channels (CC, DC, and AC), as well as between the mixed resin bed and the ion-exchange membranes within the DC compartment (DC as porous medium), continuity of ionic mass flux and Donnan equilibrium are imposed as interfacial boundary conditions (Fig. 2). These conditions couple ion transport in the electrolyte, membrane, and resin phases throughout the EDI computational domain. The corresponding expressions for mass flux continuity and Donnan equilibrium are given by [22-23]:

$$\boldsymbol{n} \cdot \boldsymbol{N}_i^m = \boldsymbol{n} \cdot \boldsymbol{N}_i^l \tag{10.0}$$

$$\Delta\varphi_D^m = \varphi^m - \varphi^l = -\frac{RT}{z_i F} ln \frac{c_i^m}{c_i^l} \tag{10.1}$$

Where the superscripts *m* and *l* refer to the membrane or liquid phase, respectively.

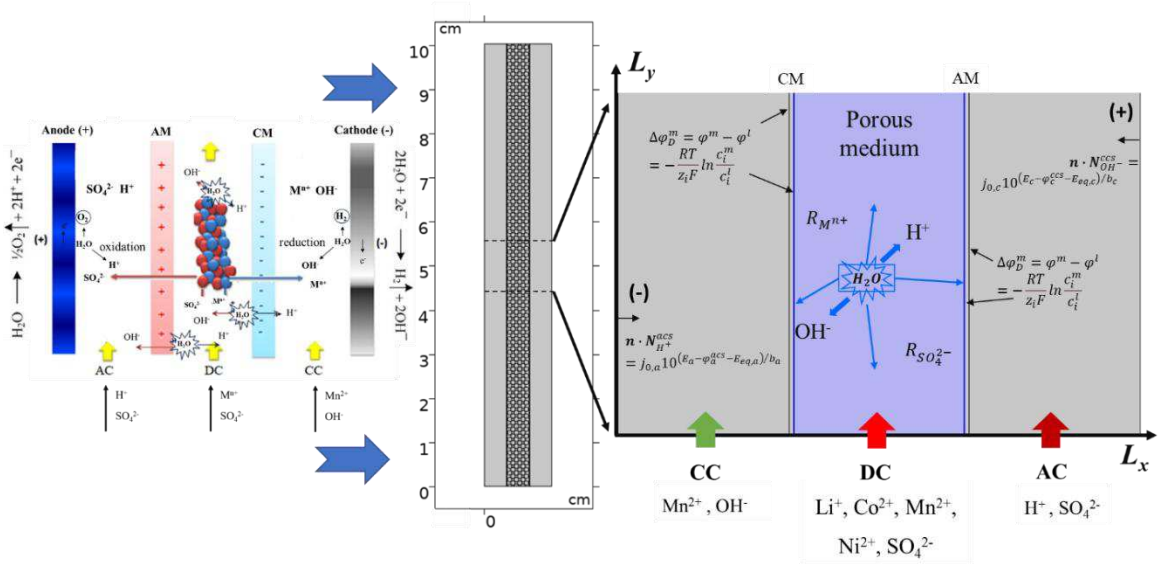


Figure 2. Schematic drawing of the 2D EDI mathematical model.

The electrochemical reactions occurring at the electrode surfaces ($x = 0$ and $x = L_x$, Fig. 2) are modeled using Tafel kinetics. Specifically, the hydrogen evolution reaction (HER) at the cathode and the oxygen evolution reaction (OER) at the anode are described by Eqs. (11.0) and (11.1), respectively [24].

$$\boldsymbol{n} \cdot \boldsymbol{N}_{H^+}^{acs} = j_{0,a} 10^{(E_a - \varphi_a^{acs} - E_{eq,a})/b_a} \tag{11.0}$$

$$\boldsymbol{n} \cdot \boldsymbol{N}_{OH^-}^{ccs} = j_{0,c} 10^{(E_c - \varphi_c^{ccs} - E_{eq,c})/b_c} \tag{11.1}$$

In Eqs. (11.0) and (11.1), E denotes the electrode potential, φ is the electrolyte potential at the electrode-electrolyte interface, E_{eq} is the equilibrium potential, b is the Tafel slope, and j_0 is the exchange current density. The subscripts a and c refer to the anode and cathode, respectively, whereas *acs* and *ccs* denote the anodic and cathodic channel solutions.

Danckwerts-type inlet boundary conditions [25] were applied at the feed entrances of the CC, DC, and AC channels ($y = 0$, Fig. 2) to prescribe the concentrations of all ionic species entering the EDI cell. The DC channel was fed with Li^+, Co^{2+}, Mn^{2+}, Ni^{2+} and SO_4^{2-}; the AC channel with H^+ and SO_4^{2-}; and the CC channel with Mn^{2+} and OH^-.

$$\boldsymbol{n} \cdot \boldsymbol{N_i^l} = \boldsymbol{n} \cdot (\boldsymbol{u} c_{0,i}) \tag{12.0}$$

$$\boldsymbol{u} c_{0,i}^l(0^-, i) = \boldsymbol{u} c_{0,i}^l(0^+, i) - Dax \frac{\partial c_i^l}{\partial z} \tag{12.1}$$

Where subscript i refers to chemical specie (Li^+, H^+, Co^{2+}, Mn^{2+}, Ni^{2+}, SO_4^{2-} and OH^-)), $c_{0,i}(0^-,i)$ is initial concentration outside channel, $c_{0,i}(0^+,i)$ is initial concentration inside channel, and Dax is axial dispersion coefficient.

3.2 Mass transfer mechanism of ion removal, water dissociation reaction and mass balance in the recirculating tanks:

The mechanism of the rate of ion exchange of sulphate ($R_{SO_4^{2-}}$) and metal ions ($R_{M^{n+}}$) on the resins porous medium (DC compartment) is described by the diffusional control model:

$$R_{SO_4^{2-}} = \frac{\partial c^d_{SO_4^{2-}}}{\partial t} = K_c \left(c^d_{SO_4^{2-}} - \frac{\left(c^d_{SO_4^{2-},0} - c^d_{SO_4^{2-}} \right)^2}{K_{eq}\left(c_{IA} - c^d_{SO_4^{2-}} \right)} \right) \tag{13.0}$$

$$R_{M^{n+}} = \frac{\partial c^d_{M^{n+}}}{\partial t} = K_c \left(c^d_{M^{n+}} - \frac{\left(c^d_{M^{n+},0} - c^d_{M^{n+}} \right)^2}{K_{eq}\left(c_{IA} - c^d_{M^{n+}} \right)} \right) \tag{13.1}$$

These equations were formulated based on the sorption kinetics of aqueous lactic acid solutions, and their derivation is similar to the reported in [26-28]. The water dissociation reaction occurring at the resin–electrolyte interface and at the contact between cation- and anion-exchange resins (DC compartment as porous medium, Fig.2) is described using the equilibrium model previously developed in [28-29]. Finally, the temporal evolution of the

concentrations of metal ions (M^{n+}) and sulfate ions (SO_4^{2-}) in the dilute and concentrate compartments during the electrodeionization process is determined by the following mass balance equation for the recirculating tanks [30]:

$$\frac{dc_{i,T}^{l}}{dt} = (c_{i,R}^{l} - c_{i,T}^{l})\frac{Q^{l}}{V_T} \tag{14.0}$$

where $c_{i,R}^{l}$ is the cross-sectional average concentration of species i at the outlet of compartment l, $c_{i,T}^{l}$ is the concentration of species i in the recirculation tank supplying compartment l of the EDI cell, Q^{l} is the volumetric flow rate, and V_T is the volume of the corresponding recirculation tank. The coupling between the recirculation tanks and the EDI model is achieved by applying Eq. (14.0) to define the inlet boundary conditions for both the dilute and concentrate compartments. Likewise, the inlet concentration of species i in each recirculation tank is obtained from the EDI model by calculating the cross-sectional average concentration at the corresponding compartment outlet, as expressed in Eq. (15.0).

$$c_{i,R}^{l} = \frac{1}{u_{av}w}\int c_{i}^{l}(\boldsymbol{u}\cdot\boldsymbol{n})\,dx \tag{15.0}$$

Where u_{av} is average velocity and w the channel width of l compartment.

3.3 Numerical solution of the EDI model

The complete set of governing equations describing the EDI model, Eqs. (4.0 to 15.0), was solved numerically using the finite element method implemented in COMSOL Multiphysics®. A structured computational mesh was employed, with three independent meshing parameters: n_y, representing the number of elements along the y-direction; $n_{x\text{-}ch}$, corresponding to the number of elements along the x-direction within each flow-channel domain; and $n_{x\text{-}mem}$, denoting the number of elements along the x-direction within each membrane domain (Fig. 3). Mesh independence was verified using a discretization consisting of approximately 100,000 domain elements and 2,200 boundary elements, corresponding to n_y = 200, $n_{x\text{-}ch}$ = 100 and $n_{x\text{-}mem}$ = 100 for which the numerical predictions of the EDI model became independent of further mesh refinement.

The operating conditions, physicochemical properties, and simulation parameters used to solve the two-dimensional EDI model at 25 °C are summarized in Table 1. The computational

performance of the model was evaluated under steady-state conditions over an applied cell voltage range of 2.0–12 V. The numerical solution required approximately 25 min 34 s to achieve convergence of the current density distribution, followed by an additional 5 min to solve the recirculation tank mass-balance equations. All simulations were performed on a workstation equipped with an Intel® Core™ i9 processor and 64 GB of RAM. The maximum memory consumption during the simulations was approximately 10 GB.

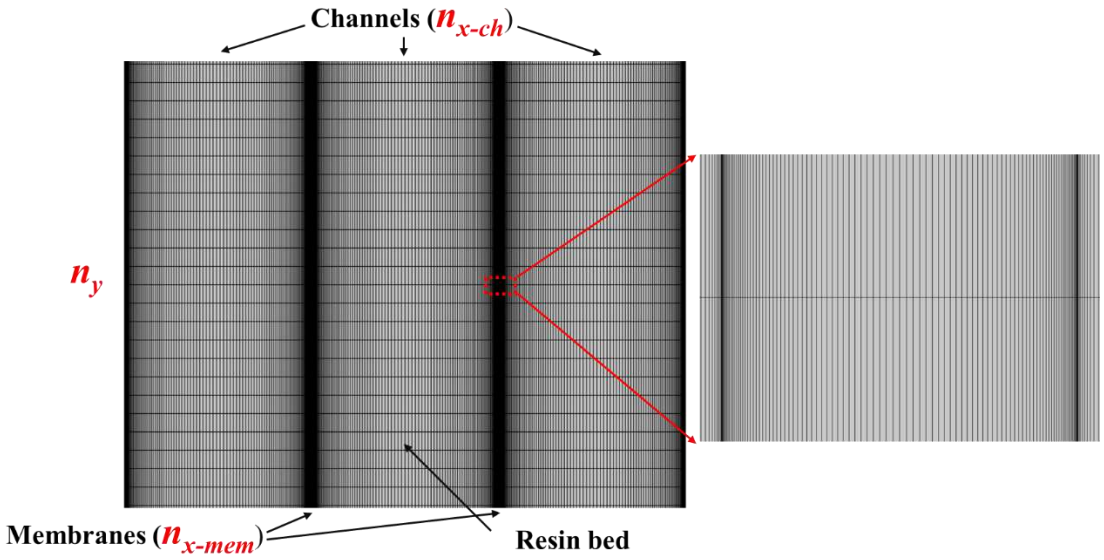


Figure 3. Structured computational mesh used for solving the EDI model.

Table 1. Model parameters and properties necessary to solve the EDI model at 25 °C.

Parameter or property	*Value*	*Note or reference*
EDI model length, L_x	1.526×10^{-2} m	a
EDI model height, L_y	1.0×10^{-1} m	a
Membrane thickness, L_{mem}	1.3×10^{-4} m	b
EDI channel length, L_{ch}	5.0×10^{-3} m	b
Capacity of membranes, ρ_{mem}	1 mol L^{-1}	c
Diffusion coefficient, D_{Mn}^{2+}	0.72×10^{-9} m^2 s^{-1}	[31]
Diffusion coefficient, D_{SO4}^{2-}	1.06×10^{-9} m^2 s^{-1}	[32]
Diffusion coefficient, D_{H}^{+}	9.312×10^{-9} m^2 s^{-1}	[28]
Diffusion coefficient, D_{OH}^{-}	5.26×10^{-9} m^2 s^{-1}	[28]

Diffusion coefficient, D_{Ni}^{2+}	0.66×10^{-9} m^2 s^{-1}	[32]
Diffusion coefficient, D_{Co}^{2+}	0.73×10^{-9} m^2 s^{-1}	[32]
Diffusion coefficient, D_{Li}^{+}	1.04×10^{-9} m^2 s^{-1}	[32]
membrane porosity, ϵ_l	0.2	[29]
membrane tortuosity, τ_l	6.35	[29]
Porosity of diluted channel (porous medium, ϵ_{DC})	0.4	[28]
Volume of liquid in recirculation tanks, V_T	0.0015 m^3	
Equilibrium potential at the anode, $E_{eq,a}$	1.23 V	[28]
Equilibrium potential at the cathode, $E_{eq,c}$	-0.83 V	[28]
Anodic Tafel slope, b_a	46 mV	[28]
Cathodic Tafel slope, b_c	-133 mV	[28]
Exchange current density at the anode, $j_{0,a}$	1.2x10^{-5} A m^{-2}	[28]
Exchange current density at the cathode, $j_{0,c}$	9.1x10^{-2} A m^{-2}	[28]

a) Calculated from geometry, laboratory-scale EDI cell used in [28].
b) Measured data.
c) Manufacturer information assuming a density of 1000 kg m^{-3}.

4. Results and discussion

4.1 Modeling of the experimental I-V curves & separation performance plots of the EDI cell

Figure 4a presents the current density–voltage (I–V) characteristics predicted by the 2D EDI model for three metallic sulfates feed concentrations (25, 50, and 100 mol m^{-3}) in the DC compartment (dilute tank reservoir, $M^{n+}SO_4$). In CC and AC compartments a feed concentration of $MnOH_2$ and H_2SO_4 with a concentration of 100 mol m^{-3} were used, respectively. The flow rate in the simulation was 30 L/h for CC and AC compartments and 10 L/h for DC compartment. The simulated polarization curves exhibit the characteristic operating regimes of electrodeionization, namely: (I) the ohmic region, (II) the transition region associated with the limiting current density (LCD), and (III) the overlimiting region. At low applied voltages (I), the current density increases almost linearly with the cell voltage, indicating that ionic transport is primarily controlled by the electrical resistance of the

electrolyte-filled resin bed. In this regime, sufficient ions are available near the ion-exchange membranes, and concentration polarization remains negligible.

As the applied voltage increases, the slope of the polarization curve progressively decreases, indicating the onset of concentration polarization at the membrane–solution, resin-solution (porous medium) interfaces. This transition corresponds to the limiting current density (II), where the ion concentration adjacent to the membrane and resins (porous medium) approaches depletion and the ion transport rate becomes controlled by mass transfer rather than by electrical conductivity. The predicted LCD shifts toward higher current densities as the feed concentration in the DC compartment increases, demonstrating that a larger ionic among delays concentration depletion at the membrane, resin (porous medium) surfaces. Consequently, the EDI model predicts limiting current densities of approximately 90, 200, and 415 A m^{-2} for feed concentrations in the DC compartment of 25, 50, and 100 mol m^{-3}, respectively.

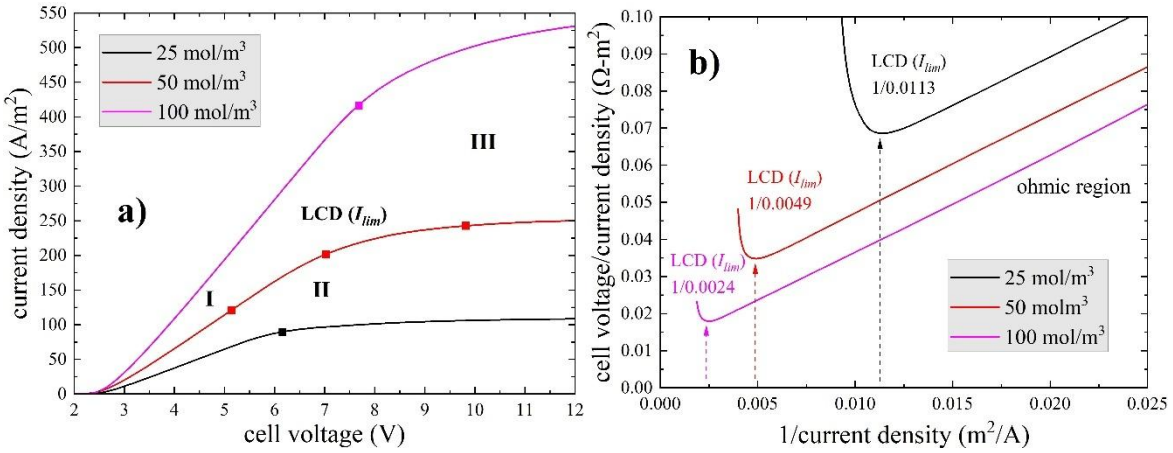


Figure 4. a) Current-voltage (I-V) curves, b) Cowan–Brown plots (LCD determination). For three metallic sulfates feed concentrations (25, 50, and 100 mol m^{-3}) in the DC channel.

Beyond the limiting current density (III), the simulations predict an overlimiting regime in which the current density continues to increase despite severe concentration polarization. This behavior is attributed to the increasing contribution of water dissociation at the interfaces between the ion-exchange resins and membranes (porous medium-membranes). The generation of H^+ and OH^- ions provide additional charge carriers that sustain electrical conduction after the available sulphate metallic ions become depleted. As a result, the EDI

process is able to operate above the classical diffusion-limited current while maintaining ionic transport through the continuous regeneration of the ion-exchange resins. This behavior is consistent with the fundamental operating mechanism of electrodeionization reported in previous studies [28], where water dissociation becomes increasingly important as electrolyte concentration near the membrane and resins approaches zero in DC compartment.

The influence of feed concentration (DC compartment) on the polarization behavior is clearly reflected by the progressive increase in current density over the entire voltage range. Higher electrolyte concentrations reduce the overall electrical resistance of the resin bed (porous medium) due to the greater availability of mobile ions, thereby increasing the electrical conductivity of the EDI (DC compartment). Consequently, higher current densities are achieved at a given applied voltage, while the transition from the ohmic to the mass-transfer-controlled regime occurs at larger current values. These results demonstrate that feed concentration in the DC compartment is one of the dominant operating variables governing the electrical response and transport capacity of the EDI cell.

To further identify the limiting current density, the Cowan–Brown method was applied to the simulated polarization data, and the corresponding results are shown in Figure 4b. This method plots the apparent electrical resistance (cell voltage/current density) as a function of the reciprocal of the current density. The limiting current density is identified from the minimum of each curve, which represents the transition between the ohmic regime and the concentration-polarization regime. The analysis predicts reciprocal current density values of approximately 0.0113, 0.0049, and 0.0024 $m^2\ A^{-1}$ for feed concentrations (DC channel) of 25, 50, and 100 mol m^{-3}, respectively, corresponding to limiting current densities close to those obtained directly from the polarization curves. The systematic displacement of the minimum toward lower reciprocal current densities confirms that increasing the feed concentration delays the onset of concentration polarization and expands the operating window before mass-transfer limitations become dominant.

The simulated I-V polarization curves and the Cowan–Brown analysis showed in Fig. 4 consistently demonstrate that electrolyte concentration in the DC compartment strongly influences the electrochemical performance of the EDI cell. Higher feed concentrations

(dilute reservoir tank) improve ionic conductivity, increase the limiting current density, reduce the relative effects of concentration polarization, and allow operation over a wider range of current densities before transport limitations become significant. These results provide valuable guidance for selecting appropriate operating conditions that maximize metallic ion removal while minimizing energy losses associated with concentration polarization.

Figure 5 illustrates the effect of the applied current density for an initial feed concentration in the DC channel of 50 mol m^{-3} on the predicted separation performance of the EDI cell process for Li^{+}, Mn^{2+}, Co^{2+}, and Ni^{2+}. Figure 5a presents the normalized concentration increase $((c-c_0)/c_0)$ as function of time in the concentrate reservoir tank, whereas Fig. 5b shows the corresponding normalized concentration decrease (c/c_0) as function of time in the dilute reservoir tank, both for 10 h of EDI operation. Three operating regimes were considered in the simulation, corresponding to region I (sub-limiting current density, ohmic region), the limiting current density (LCD), and region III (over-limiting current density), as showed in Fig. 5a for the feed concentration of 50 mol m^{-3} in the DC channel (red line).

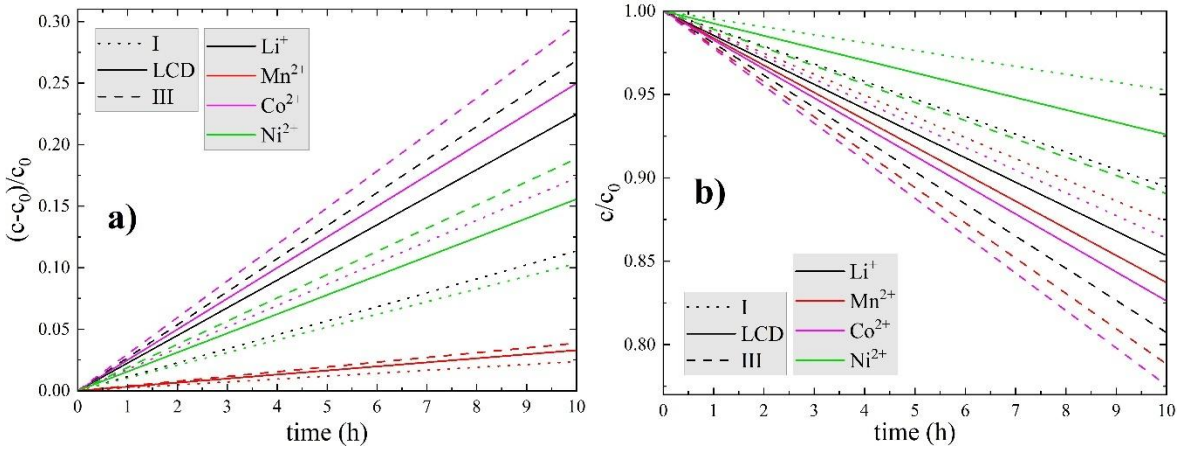


Figure 5. Time-dependent normalized metallic concentration in the recirculation tanks for three current densities applied at 50 mol m^{-3} in the DC compartment. a) concentrate reservoir tank (cathodic channel), b) dilute reservoir tank (anodic channel).

The simulation results demonstrate that increasing the applied current density significantly enhances ionic transport from the dilute channel toward the concentrate channel of the EDI cell. For all ionic species, the highest enrichment rates are obtained under over-limiting current conditions (region III), while the lowest enrichment occurs in region I. This behavior

is directly attributed to the increase in electromigration driving force, which promotes faster ion transport through the ion-exchange membranes and resins (porous medium). Consequently, the concentration of all metal ions increases almost linearly with time in the concentrate reservoir tank, while a corresponding decrease is observed in the dilute reservoir tank.

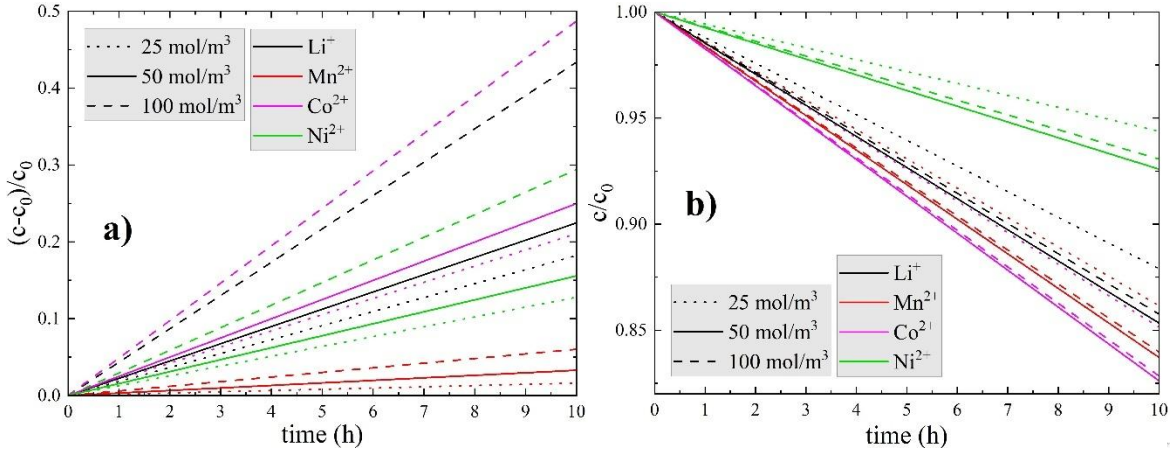
The EDI model also predicts clear differences among the transported ions. Co^{2+} exhibits the highest accumulation in the concentrate reservoir tank and the largest depletion in the dilute reservoir tank throughout the simulated period (10 h). Li^{+} presents the second highest transport rate, followed by Ni^{2+}, whereas Mn^{2+} consistently shows the lowest transport efficiency. These differences indicate that the transport behavior is governed not only by the applied electric field but also by the intrinsic physicochemical properties of each ion, including ionic mobility, membrane-resin transport characteristics, and competition among the multicomponent ionic species.

The separation performance becomes progressively more pronounced as the current density increases from region I to the over-limiting regime. Under these conditions, the larger electrical driving force accelerates ion migration, resulting in higher recovery efficiencies within the same operating time. Therefore, the simulations suggest that operating above the limiting current density substantially improves metal-ion recovery, although practical operation should also consider possible concentration polarization and increased energy consumption associated with over-limiting conditions.

Figure 6 presents the effect of the initial feed concentration of sulphate metal ions in the dilute channel on the predicted time-dependent separation performance of the EDI cell operating within the limiting current density (LCD) regime. Three feed concentrations, 25, 50, and 100 mol m^{-3}, were simulated. Figure 6a shows time-dependent normalized concentration increase in the concentrate reservoir tank, whereas Fig. 6b illustrates time-dependent normalized concentration decrease in the dilute reservoir tank during 10 h of EDI operation.

The simulation results indicate that increasing the initial concentration in the dilute stream enhances the overall ion transport toward the concentrate reservoir tank. For every ionic

546 species, the highest enrichment is obtained at an initial concentration of 100 mol m^{-3}, while
547 the lowest enrichment corresponds to 25 mol m^{-3}. The greater ion availability in the feed DC
548 solution provides a larger concentration of charge carriers, increasing the electromigration
549 flux and promoting faster accumulation in the concentrate reservoir tank



550

551 **Figure 6.** Time-dependent normalized metallic concentration in the recirculation tanks for
552 three initial feed concentration of sulphate metal ions in the dilute channel obtained in the
553 LCD condition. a) concentrate reservoir tank (cathodic channel), b) dilute reservoir tank
554 (anodic channel).

555 A similar trend is observed in the dilute reservoir tank, where higher initial concentrations
556 produce a more rapid decrease in normalized concentration. Although all ions exhibit
557 continuous depletion throughout the simulation, the depletion rate varies according to the
558 ionic species. Co^{2+} again shows the greatest transport efficiency, followed by Li^{+}, while Ni^{2+}
559 exhibits the slowest concentration decrease. Mn^{2+} maintains an intermediate transport
560 behavior. These differences demonstrate that competitive ion transport remains significant
561 even when the feed concentration in DC compartment is modified, indicating that ionic
562 mobility and membrane-resin selectivity continue to control the separation process.

563 The simulations results showed in Figs. 5 and 6 reveal that both the applied current density
564 and the initial feed concentration in the DC compartment strongly influence EDI
565 performance. Higher feed concentrations increase the available ionic flux, while higher
566 current densities strengthen the electromigration driving force. The combined effect of these
567 operating parameters results in faster ion removal from the dilute reservoir tank and greater
568 accumulation in the concentrate reservoir tank, confirming that the developed EDI model

proposed in this work successfully captures the expected EDI transient behavior of multicomponent ion transport under different operating conditions.

Figure 7 presents the influence of the initial feed electrolyte concentration in the anodic and cathodic channels on the electrochemical performance of the EDI cell at the LCD condition obtained with the initial feed electrolyte concentration in the dilute channel of 50 mol m^{-3}. Figure 7a shows the simulated current density–voltage (I–V) curves for feed electrolyte concentrations of 50, 100, and 200 mol m^{-3} in the anodic and cathodic channels, while Fig. 7b shows the corresponding Cowan–Brown plots used to determine the limiting current density (LCD). The simulated I–V curves indicate that increasing the electrolyte concentration in the electrode compartments substantially improves the electrical conductivity of the EDI cell. At a given cell voltage, the current density increases consistently with increasing electrolyte concentration, reaching approximately 200, 250, and 380 A m^{-2} at 12 V for feed concentrations of 50, 100, and 200 mol m^{-3}, respectively. This behavior is attributed to the larger concentration of ionic charge carriers available in the electrode channels, which reduces the ohmic resistance of the electrolyte and facilitates charge transport between the electrode channels and the ion-exchange membranes. Consequently, the EDI cell is capable of operating at higher current densities before concentration polarization becomes significant.

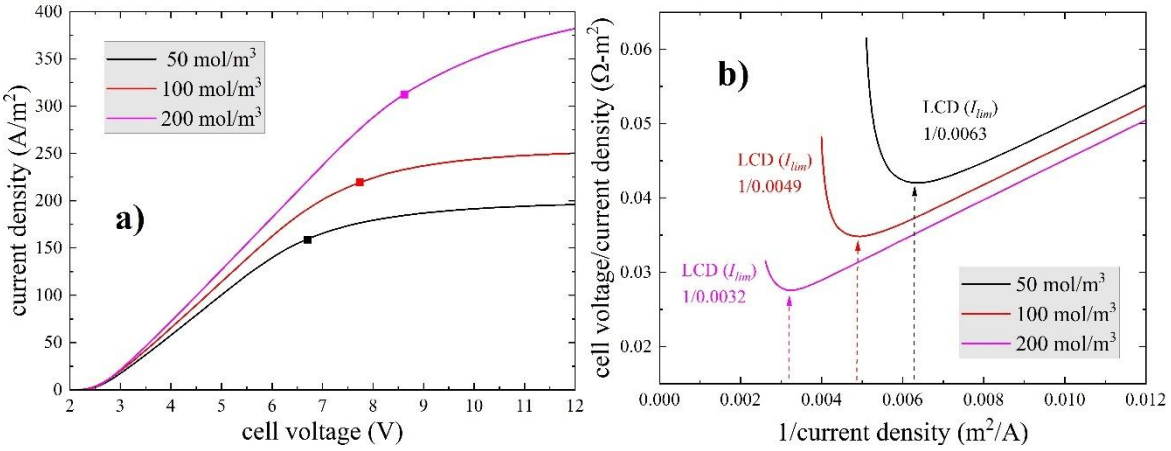


Figure 7. a) Current-voltage (I-V) curves, b) Cowan–Brown plots (LCD determination). For three feed concentrations (50, 100, and 200 mol m^{-3}) in the anodic and cathodic channels, maintaining the DC channel feed concentration at 50 mol m^{-3}.

The Cowan–Brown analysis shown in Fig. 7b confirms this trend by predicting a progressive increase in the limiting current density as the electrolyte concentration in the anodic and cathodic channels increases. The estimated LCD values rise from approximately 159 A m^{-2} for 50 mol m^{-3}, 204 A m^{-2} and 313 A m^{-2} for 100 and 200 mol m^{-3}, respectively, corresponding to the inverse current density values indicated in Fig 7b. The displacement of the minimum point toward lower values of (1/current density) demonstrates that higher electrolyte concentrations in the anodic and cathodic channels delay the onset of concentration polarization, thereby extending the operating region where ion transport remains controlled by electromigration rather than by mass-transfer limitations. These results indicate that increasing the ionic strength of the electrode compartments enlarges the feasible operating window of the EDI cell and allows higher current densities to be applied without reaching the limiting current condition.

Figure 8 illustrates the corresponding effect of the anodic and cathodic channel electrolyte concentration on the predicted metal recovery performance. Figure 8a presents the normalized concentration increase, $((c-c_0)/c_0)$, in the concentrate reservoir (cathodic channel), whereas Fig. 8b shows the normalized concentration remaining, (c/c_0), in the dilute reservoir (anodic channel) during 10 h of EDI operation for 50, 100, and 200 mol m^{-3} of anodic and cathodic channel electrolyte concentrations and maintaining a concentration of 50 mol m^{-3} in the DC compartment.

The simulations reveal that increasing the electrolyte concentration in the electrode channels enhances the separation efficiency for all metallic ions. The highest enrichment in the concentrate reservoir is consistently obtained with an electrolyte concentration of 200 mol m^{-3}, whereas the lowest enrichment corresponds to 50 mol m^{-3}. The higher electrolyte concentration reduces the electrical resistance within the electrode compartments, resulting in a more uniform electric field and a larger electromigration driving force across the ion-exchange membranes. Consequently, the transport rates of Li^{+}, Co^{+2}, Mn^{2+}, and Ni^{2+} are significantly increased throughout the simulation period.

Differences in transport behavior among the metallic ions are also observed. Co^{2+} exhibits the highest accumulation in the concentrate reservoir under all simulated conditions,

followed by Li^{+}, whereas Ni^{2+} presents the lowest enrichment. Mn^{2+} shows only a limited concentration increase compared with the other ions. These differences remain consistent regardless of the electrolyte concentration, indicating that the relative transport selectivity is primarily governed by the intrinsic transport properties of each ionic species, while the electrolyte concentration of the electrodes compartments mainly affects the magnitude of the ionic flux.

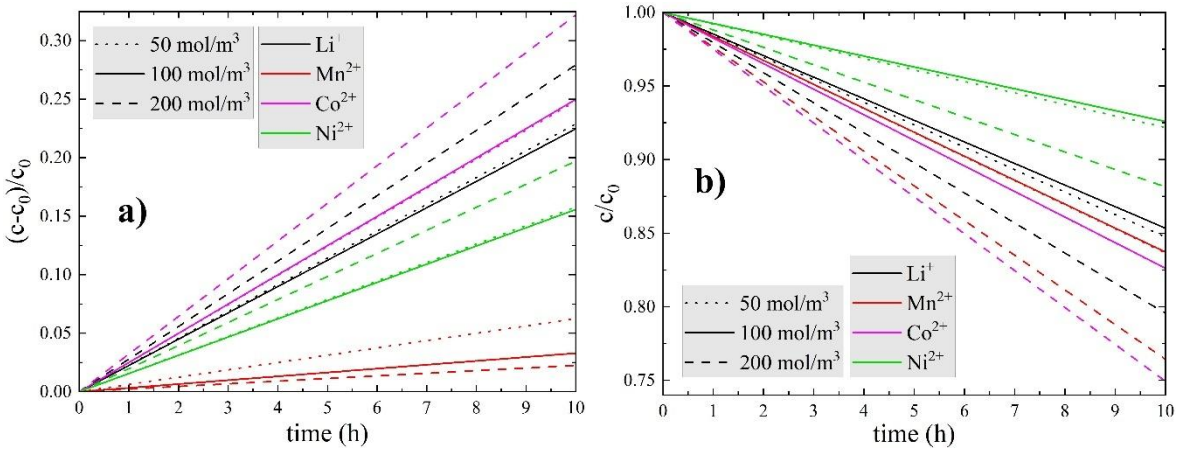


Figure 8. Time-dependent normalized metallic concentration in the recirculation tanks for three initial concentrations in the anodic and cathodic channels, maintaining the DC channel feed concentration at 50 mol m^{-3}. a) concentrate reservoir tank (cathodic channel), b) dilute reservoir tank (anodic channel).

The concentration profiles in the dilute reservoir tank as function of time, shown in Fig. 8b, exhibit the complementary behavior. Increasing the feed electrolyte concentration in the electrode channels, accelerates the depletion of all metallic ions from the dilute stream, with the most pronounced concentration decrease occurring at 200 mol m^{-3}. Co^{2+} again presents the highest removal rate, whereas Ni^{2+} remains the least depleted species. The nearly linear concentration variations predicted over the simulated operating period suggest that stable electromigration conditions are maintained, without abrupt changes associated with severe concentration polarization.

The simulation results presented in Figures 7 and 8 demonstrate that the electrolyte concentration in the anodic and cathodic channels is an important operating parameter governing EDI performance. Increasing the electrolyte concentration simultaneously reduces cell resistance, increases the limiting current density, and enhances metallic ion transport

643 from the dilute to the concentrate reservoirs tanks. These improvements lead to higher
644 recovery rates while extending the operating range below the limiting current density,
645 providing more favorable conditions for efficient continuous recovery of lithium and
646 transition metals from multicomponent sulfate solutions.

647 *4.2 EDI cell performance for lithium recovery*

648 The performance of the EDI cell for lithium recovery can be assessed in terms of lithium
649 removal from the dilute stream, lithium enrichment in the concentrate stream, and the relative
650 transport of Li^+ with respect to competing transition-metal ions. These parameters are
651 particularly relevant for multicomponent sulfate leachates, where Li^+ coexists with Co^{2+},
652 Ni^{2+}, and Mn^{2+} and where the simultaneous transport of metallic species determines the
653 effectiveness of the separation process. In this regard, the EDI performance is governed by
654 the coupled effects of the applied electric field, feed concentration, ionic transport properties,
655 and membrane–resin interactions.

656 The results obtained with the 2D EDI model demonstrate that the applied current density is
657 a key parameter controlling the rate of lithium and metal transport. At a fixed initial
658 concentration of 50 mol m^{-3} in the dilute compartment, increasing the current density from
659 the ohmic region to the limiting and over-limiting regimes progressively enhances the
660 migration of Li^+ from the dilute reservoir toward the concentrate reservoir tanks. Under over-
661 limiting conditions, the highest enrichment rates are obtained for all metallic species as a
662 consequence of the stronger electromigration driving force. Thus, increasing the current
663 density accelerates lithium removal and accumulation within the same operating period.
664 However, operation at excessively high current densities should be carefully considered
665 because the enhanced transport rate may be accompanied by increased electrical energy
666 requirements and stronger contributions from water dissociation.

667 The simulations also reveal that lithium transport is strongly affected by the initial
668 concentration of the metallic sulfate solution. At the limiting current density, increasing the
669 initial concentration in the dilute compartment from 25 to 100 mol m^{-3} increases the
670 accumulation of all metallic ions in the concentrate reservoir and accelerates their depletion
671 from the dilute reservoir. The greater availability of ionic charge carriers increases the

electromigration flux and allows faster transport through the membrane–resin system. Therefore, a higher feed concentration favors lithium removal and enrichment while simultaneously increasing the transport of the competing transition-metal ions.

An important aspect of the EDI performance is the relative selectivity toward lithium in the presence of divalent transition metals. The model predicts distinct transport rates for the different ionic species, with Co^{2+} exhibiting the highest accumulation in the concentrate reservoir, followed by Li^{+}, whereas Ni^{2+} and Mn^{2+} exhibit lower transport rates. This behavior is maintained under the different operating conditions evaluated, indicating that the separation is not determined exclusively by the applied electric field. Instead, the relative transport of each species results from the combined effects of ionic transport properties, membrane–resin characteristics, and competitive migration among the multicomponent ions. Consequently, although increasing the electrical driving force improves lithium recovery, it also promotes the simultaneous transport of Co^{2+} and the other transition-metal ions, which must be considered when assessing lithium selectivity.

The electrolyte concentration in the anodic and cathodic compartments provides an additional means of improving EDI performance. Increasing this concentration from 50 to 200 mol m^{-3} substantially increases the electrical conductivity of the electrode compartments and shifts the limiting current density from approximately 159 to 313 A m^{-2}. At the same time, higher electrolyte concentrations enhance the transport of Li^{+} and the competing transition-metal ions from the dilute to the concentrate reservoir. The highest enrichment and depletion rates are obtained at 200 mol m^{-3}, indicating that increasing the ionic strength of the electrode compartments reduces cell resistance and strengthens the effective electromigration driving force across the ion-exchange membranes.

Nevertheless, the results indicate that increasing the electrolyte concentration of the electrode compartments primarily affects the magnitude of the ionic flux rather than the relative transport order among the metallic species. Co^{2+} consistently exhibits the highest accumulation in the concentrate reservoir, followed by Li^{+}, whereas Ni^{2+} shows the lowest enrichment and Mn^{2+} exhibits an intermediate or comparatively limited transport behavior. A similar trend is observed in the dilute reservoir, where Co^{2+} presents the highest removal

rate and Ni^{2+} the lowest. The persistence of this transport hierarchy over the investigated operating conditions suggests that the intrinsic transport characteristics of the ions play a major role in determining the relative selectivity of the EDI cell.

From a process-performance perspective, these results demonstrate that lithium removal efficiency and lithium concentration factor can be enhanced by increasing both the applied current density and the initial electrolyte concentration. However, these improvements are accompanied by enhanced transport of Co^{2+}, Mn^{2+}, and Ni^{2+}. Therefore, maximum lithium recovery does not necessarily correspond to maximum lithium selectivity. An appropriate operating condition should instead provide a balance between lithium transport, competing-metal transport, concentration polarization, and electrical energy consumption. The polarization analysis indicates that increasing the feed concentration increases the limiting current density and extends the operating window before mass-transfer limitations become dominant, providing an additional criterion for selecting the operating conditions for lithium recovery.

Accordingly, the principal performance indicators for the EDI recovery of lithium from sulfate leachates should include lithium removal efficiency, lithium concentration factor, current efficiency, specific energy consumption, and lithium selectivity relative to Co^{2+}, Ni^{2+}, and Mn^{2+}. The present simulations directly demonstrate the effects of operating conditions on lithium removal and enrichment and provide the basis for evaluating the relative transport of lithium and transition metals. Although current efficiency and specific energy consumption were not explicitly quantified in the present simulations, they should be incorporated in future optimization analyses and experimental studies to identify operating conditions that maximize lithium recovery while limiting energy demand and undesirable transition-metal co-transport. In this regard, the results presented in Figures 5–8 establish that the EDI system provides a controllable platform for continuous lithium transport and concentration from multicomponent sulfate solutions, while also highlighting the need to optimize the electromigration driving force against competitive ion transport and energy requirements.

The model predicts that increasing the current density intensifies the transport of metal species from the diluate compartment to the concentrate compartment. However, an increase in the total ionic flux does not necessarily imply improved selective separation. Under the simulated conditions, Co^{2+} exhibits the greatest accumulation in the concentrate, whereas Li^{+} ranks second. This behavior indicates that the membrane–resin configuration considered here does not, by itself, promote preferential lithium transport over cobalt. Accordingly, the system response should be interpreted as the co-concentration of metal cations. Demonstrating Li^{+} selectivity will require calculating separation factors from molar fluxes and feed compositions, and evaluating monovalent-selective cation-exchange membranes, lithium-affine resins, or an upstream step for removing Co^{2+}, Ni^{2+}, and Mn^{2+}.

4.3 Literature context and relevance to the EDI model

The available literature listed in Table 2 provides consistent support for the physical interpretation of the present EDI model for lithium recovery from multicomponent lithium-ion battery (LIB) leachates. Previous EDI studies have demonstrated that the cell current increases with the applied voltage and that the current–voltage (I–V) response can be associated with distinct ohmic, concentration-polarization/limiting-current, and overlimiting regimes, the latter being related, under sufficiently high applied potentials, to water dissociation and enhanced H^{+}/OH transport. In particular, Demir *et al.* [14] demonstrated efficient Li^{+} removal using EDI and showed that applied voltage, electrolyte concentration, and competing cations significantly influence lithium transport and current distribution. Although this study employed a simplified Li^{+}-containing solution, its results provide a direct benchmark for the lithium-specific behavior of the present EDI system. For the electrical interpretation of the I–V response, Bouhidel and Lakehal [33] reported three approximately linear regions in an EDI current–voltage characteristic and identified a water-dissociation threshold under their experimental conditions. This provides a useful framework for interpreting the low-voltage ohmic regime, concentration-polarization/limiting-current transition, and high-voltage overlimiting regime of the present model.

More recent electrodialysis studies using NMC and NCA battery leachates [34-36] have further demonstrated Li^{+} transport and selective recovery in the presence of Co^{2+}, Ni^{2+}, and

Mn^{2+}, confirming the importance of competitive multivalent-ion transport in realistic LIB-derived solutions. Studies involving Li_2SO_4 and $LiCoO_2$ solutions obtained from hydrometallurgical LIB recycling [37, 38] are also particularly relevant to the present sulfate-based system because they highlight the coupled roles of sulfate transport, membrane voltage losses, and water dissociation. Accordingly, the current predicted by the present multicomponent EDI model should be interpreted as the combined contribution of Li^+, Co^{2+}, Ni^{2+}, Mn^{2+}, SO_4^{2-}, and, depending on the compartment and operating conditions, H^+ and OH^- rather than as a lithium-only response. The available literature therefore supports the proposed interpretation of the simulated I–V characteristics while also highlighting an important research gap: few studies have simultaneously considered a realistic Li–Co–Ni–Mn battery-leachate composition, ion-exchange resins, detailed ionic transport, and complete cell I–V behavior within an EDI architecture. The present model addresses this gap by coupling multicomponent Nernst–Planck transport, electroneutrality, membrane/resin phase behavior, concentration polarization, and electrode reactions, providing a mechanistic framework for predicting the electrical response and selective lithium transport in EDI systems applied to LIB recycling.

Table 2. Literature benchmark

Reference	**System / feed**	**Main species**	**Process**	**Main contribution to EDI model**
[14] Demir *et al.* (2023), ACS Omega, DOI:10.1021/acsomega.2c08095	Li-containing aqueous solution	Li^+, competing mono-/divalent cations	EDI	Direct EDI benchmark for Li^+ transport; effect of voltage, flow rate, competing ions, and electrode-electrolyte concentration.
[33] Bouhidel & Lakehal (2006), Desalination, DOI:10.1016/j.desal.2005.08.027	EDI water-treatment system	Generic ionic solution	EDI	Direct I–V benchmark; three approximately linear regions and experimentally observed water-dissociation threshold.
[34] Foo *et al.* (2024), Environmental Science & Technology, DOI:10.1021/acs.est.4c06033	NMC battery leachate	Li^+, Co^{2+}, Ni^{2+}, Mn^{2+}	Selective ED / BMED	Strong multicomponent benchmark for Li^+ selectivity and competitive transport in battery leachates.
[35] Xing & Srinivasan (2023), Chemical Engineering Journal, DOI:10.1016/j.cej.2023.145306	Industrial LCO, Ni-rich and NMC leachates	Li and transition metals	ED with bipolar membrane	Demonstrates Li recovery from real LIB leachates; useful benchmark for realistic feed complexity, purity, and recovery.

[36] Lima *et al.* (2025), Environmental Technology, DOI:10.1080/09593330.2025.2451781	Synthetic NCA battery leachate	Li^+, Ni^{2+}, Co^{2+}, Al^{3+}	ED	Quantifies current-density effects and migration of mono-, di-, and trivalent cations; supports multicomponent transport interpretation.
[37] J. Zhu *et al.* (2025), Separation and Purification Technology, DOI:10.1016/j.seppur.2024.128715	LIB-derived Li_2SO_4 solution	Li^+, SO_4^{2-}, H+/OH−	BMED	Directly relevant to sulfate chemistry, water dissociation, voltage losses, current density, and LiOH recovery.
[38] Cerrillo-Gonzalez *et al.* (2020), Applied Sciences, DOI:10.3390/app10072367	$LiCoO_2$ hydrometallurgical leachate	Li^+, Co^{2+}	Hydrometallurgical–ED	Connects LIB leaching with ED transport and Li/Co recovery; useful for linking upstream leaching and electromembrane separation.

Conclusions

A two-dimensional model was developed to analyze the electrochemical behavior and ionic transport in an EDI cell fed with a multicomponent sulfate solution. The model relates the current–voltage response to the time evolution of concentrations in the diluate and concentrate compartments. The simulated polarization curves exhibit ohmic, limiting-current, and overlimiting regions. Increasing the feed concentration in the diluate compartment from 25 to 100 mol m^{-3} raises the estimated limiting current density from approximately 90 to 415 A m^{-2}, reflecting the effect of concentration on conductivity and concentration polarization.

Increasing the current density and the electrolyte concentration in the electrode compartments enhances the transport of Li^+, Co^{2+}, Ni^{2+}, and Mn^{2+} toward the concentrate compartment. However, Co^{2+} exhibits the greatest accumulation under the conditions investigated, followed by Li^+. Thus, the results do not demonstrate intrinsic lithium selectivity; rather, they indicate that the modeled EDI configuration can promote the co-concentration of metal species. The relative order of Ni^{2+} and Mn^{2+} should be established from the quantitative data and reported consistently in the figures, discussion, and conclusions.

The model provides a tool for exploring transport trends and electrical response, but assessing its suitability for lithium recovery requires experimental validation using multicomponent solutions representative of real battery leachates. Lithium recovery, concentration factor, purity, separation factors, current efficiency, and specific energy consumption should also be quantified. Finally, the formulation should explicitly address competitive resin exchange, aqueous speciation and possible metal precipitation at elevated pH, and the actual composition of the anolyte and catholyte.

The electrolyte concentration in the anodic and cathodic compartments was identified as another important operating variable. Increasing the electrode-compartment electrolyte concentration from 50 to 200 mol m^{-3} substantially increased the electrical conductivity of the EDI cell and shifted the limiting current density from approximately 159 to 313 A m^{-2}. In addition, higher electrode-compartment concentrations increased the transport rates of all investigated metallic ions and enhanced their accumulation in the concentrate reservoir. Thus, increasing the ionic strength of the electrode compartments can extend the feasible operating window of the EDI cell while improving the overall metallic-ion transport rate.

From the perspective of lithium recovery, the simulation results obtained in this work demonstrate that EDI provides an effective means of continuously removing and concentrating Li^{+} from multicomponent sulfate solutions. However, the simultaneous transport of Co^{2+}, Mn^{2+}, and Ni^{2+} demonstrates that maximizing lithium recovery and maximizing lithium selectivity are not necessarily equivalent objectives. In particular, the higher transport rate predicted for Co^{2+} indicates that additional optimization of membrane–resin properties and operating conditions is required to enhance lithium selectivity relative to competing divalent ions. Therefore, the developed model here provides a useful tool for identifying operating conditions that balance lithium transport, transition-metal co-transport, concentration polarization, and electrical performance.

The simulation results in this work establish the capability of the developed 2D EDI model to capture the principal electrochemical and transient transport phenomena governing multicomponent ion separation. The combined analysis of polarization behavior and reservoir concentration profiles provides a quantitative basis for selecting feed and electrode-

compartment concentrations and current densities for EDI operation. Future work should incorporate quantitative evaluation of lithium removal efficiency, lithium concentration factor, current efficiency, specific energy consumption, and lithium selectivity, together with experimental validation under multicomponent sulfate-leach conditions. Such an integrated performance analysis will be essential for optimizing the EDI process toward energy-efficient and selective lithium recovery from spent lithium-ion battery leachates.

CRediT authorship contribution statement

I.J. González-Panzo: Investigation, Methodology, Formal analysis, Visualization, Writing-original draft, Software. **R.A. Bustamante-Rendon:** Investigation, Visualization, Methodology, Writing – review & editing. **F.J. Almazán-Ruiz:** Investigation, Software, Methodology, Writing – review & editing. **Gustavo Aparicio-Mauricio**: Investigation, Software, Methodology, Writing – review & editing. **María Aurora Martínez-Trujillo**: Conceptualization, Validation, Supervision, Writing – review & editing. **Martín R. Cruz-Díaz:** Conceptualization, Validation, Supervision, Funding acquisition, Writing – review & editing.

Declaration of competing interest

The authors declare that they have no known competing financial interests or personal relationships that could have appeared to influence the work reported in this paper.

Acknowledgments

The authors express their gratitude to SECIHTI for the financial support provided for the development of this research through the project No. CBF 2023-2024-741 and TecNM for the financial support provided under projects numbers: 20239.24-PD, 25945.26-PD and 26389.26-PD. Isidro J. González-Panzo would like to thank to CONACYT for extending postdoctoral scholarship according to ESTANCIAS POSDOCTORALES POR MEXICO 2022(1), Continuidad de Estancia Posdoctoral Académica (3) 2022. The co-author R.A.

Bustamante-Rendon, gratefully acknowledges the Mexican Council of Science and Technology (COMECYT) for the support provided through its Research Fellowship Program (Programa Cátedra), under grant number **CAT2025-0014**, which contributed to the development of this research.

References

[1] M. Rezaei *et al.*, A review of lithium-ion battery recycling for enabling a circular economy, Journal of Power Sources, 630 (2025) 236157, https://doi.org/10.1016/j.jpowsour.2024.236157

[2] Gaolei Wei, Yuxuan Liu, Binglei Jiao, Nana Chang, Mengting Wu, Gangfeng Liu, Xiao Lin, XueFei Weng, Jinxing Chen, Liang Zhang, Chunling Zhu, Guiling Wang, Panpan Xu, Jiangtao Di, Qingwen Li, Direct recycling of spent Li-ion batteries: Challenges and opportunities toward practical applications, iScience, 26(9) (2023) 107676, https://doi.org/10.1016/j.isci.2023.107676

[3] Yonglin Yao, Meiying Zhu, Zhuo Zhao, Bihai Tong, Youqi Fan, and Zhongsheng Hua, Hydrometallurgical Processes for Recycling Spent Lithium-Ion Batteries: A Critical Review, ACS Sustainable Chemistry & Engineering, 6(11) (2018) 13611-13627, https://doi.org/10.1021/acssuschemeng.8b03545

[4] E. Asadi Dalini, Gh. Karimi, S. Zandevakili, & M. Goodarzi, A Review on Environmental, Economic and Hydrometallurgical Processes of Recycling Spent Lithium-ion Batteries, Mineral Processing and Extractive Metallurgy Review, 42(7) (2021) 451-472, https://doi.org/10.1080/08827508.2020.1781628

[5] Mingxian Zhou, Bang Li, Jia Li, and Zhenming Xu, Pyrometallurgical Technology in the Recycling of a Spent Lithium Ion Battery: Evolution and the Challenge, ACS ES&T Engineering, 1(10) (2021) 1369-1382, https://doi.org/10.1021/acsestengg.1c00067

[6] J. Mušović, A. Jocić, A. Dimitrijević, Recent Advances in Leaching of Lithium-Ion Battery Cathode Materials Using Deep Eutectic Solvents and Ionic Liquids: Efficiency, Mechanisms, and Challenges. Processes 13 (2025) 4015, https://doi.org/10.3390/pr13124015

[7] P. Hubert, A. Vanderbruggen, S. Jradi, A. Chagnes, Selective metal recovery: Innovating leaching of LFP-NMC cathode mixtures from spent lithium-ion batteries, Sustainable Materials and Technologies, 46 (2025) e01658, https://doi.org/10.1016/j.susmat.2025.e01658

[8] H.M. Akbar, S. Habib, R. Akoumeh, *et al.*, Lithium Extraction Methodology and Recovery from Conventional Resources: A Critical Review, Water Air Soil Pollut 236 (2025) 723, https://doi.org/10.1007/s11270-025-08382-4

[9] A. Roa, S. Butylina, J. López, J.L. Cortina, S. Virolainen, M. Mänttäri, Lithium recovery from battery waste leachate by nanofiltration: Impact of types of leaching acid and alkaline on permeability of lithium ions, Separation and Purification Technology, 360 (2025) 130821, https://doi.org/10.1016/j.seppur.2024.130821

[10] F. Wu, K.R. Shivakumar, K.O. Konhauser, *et al.*, Lithium resources and novel strategies for their extraction and purification. npj Mater. Sustain. 3 (2025) 30, https://doi.org/10.1038/s44296-025-00069-5

[11] J. Park, J. Lee, I.T. Shim, E. Kim, S.H. Nam, J.W. Koo, T.M. Hwang, Electrochemical Direct Lithium Extraction: A Review of Electrodialysis and Capacitive Deionization Technologies, Resources, 14 (2025) 27, https://doi.org/10.3390/resources14020027

[12] Muslim, D. S., R. Ghanoum, N. N. Mohammed, *et al.*, Sustainable Lithium Recovery From Aqueous Sources Using Advanced Extraction Technologies: A Comprehensive Review, Water Environment Research, 98(3) (2026) e70342, https://doi.org/10.1002/wer.70342

[13] X. Li, *et al.*, Membrane-based technologies for lithium recovery from water lithium resources: A review, Journal of Membrane Science, (2019) 591 117317, https://doi.org/10.1016/j.memsci.2019.117317

[14] Gülseren Demir, Ayşe Nur Mert, and Özgür Arar, Utilization of Electrodeionization for Lithium Removal, ACS Omega, 8(20) (2023) 17583-17590, https://doi.org/10.1021/acsomega.2c08095

[15] H.B. Ulusoy Erol, C.N. Hestekin, J.A. Hestekin, Effects of Resin Chemistries on the Selective Removal of Industrially Relevant Metal Ions Using Wafer-Enhanced Electrodeionization, Membranes (2021) 11 45, https://doi.org/10.3390/membranes11010045

[16] Roman Kodým, Dalimil Šnita, Karel Bouzek, Chapter 12 - Mathematical Modeling of Electromembrane Processes, Editor(s): Angelo Basile, Efrem Curcio, Inamuddin, Current Trends and Future Developments on (Bio-) Membranes, Elsevier (2019) 285-326, https://doi.org/10.1016/B978-0-12-813551-8.00012-7

[17] John R. Fanchi, Chapter 9 - Fluid Flow Equations, Editor(s): John R. Fanchi, Shared Earth Modeling, Butterworth-Heinemann (2002) 150-169, https://doi.org/10.1016/B978-075067522-2/50009-4

[18] Syed Ahmad Imtiaz, Chapter 2 - Model equations and modeling methodology, Editor(s): Syed Ahmad Imtiaz, Modelling of Chemical Process Systems, Elsevier (2023) 21-49, https://doi.org/10.1016/B978-0-12-823869-1.00004-1

[19] Benjamin Janotta, Maximilian Schalenbach, Hermann Tempel, Rüdiger-A. Eichel, An assessment of electroneutrality implementations for accurate electrochemical ion transport models, Electrochimica Acta, 508 (2024) 145280, https://doi.org/10.1016/j.electacta.2024.145280

[20] Dragan Poljak, Mario Cvetković, Chapter 2 - Theoretical Background: an Outline of Computational Electromagnetics (CEM), Editor(s): Dragan Poljak, Mario Cvetković, Human Interaction with Electromagnetic Fields, Academic Press, (2019) 21-52, https://doi.org/10.1016/B978-0-12-816443-3.00010-8

[21] Aldo Ledesma-Durán, S. I. Hernández, and Iván Santamaría-Holek, Relation between the porosity and tortuosity of a membrane formed by disconnected irregular pores and the spatial diffusion coefficient of the Fick-Jacobs model, Phys. Rev. E 95 (2017) 052804, https://doi.org/10.1103/PhysRevE.95.052804

[22] Yousef Haseli, Chapter One - Fundamental concepts, Editor(s): Yousef Haseli, Entropy Analysis in Thermal Engineering Systems, Academic Press, (2020) 1-11, https://doi.org/10.1016/B978-0-12-819168-2.00001-5

[23] H. Strathmann, MEMBRANE SEPARATIONS | Electrodialysis, Editor(s): Ian D. Wilson, Encyclopedia of Separation Science, Academic Press, (2000) 1707-1717, https://doi.org/10.1016/B0-12-226770-2/05131-0

[24] C.M.A. Brett, A.M.O. Brett, Electrochemistry, Principles, Methods, and Applications, Oxford University Press, New York, 1993, pp. 416–419.

[25] Martín R. Cruz-Díaz, Alejandra Laureano, Francisca A. Rodríguez, Luis F. Arenas, Joep J. H. Pijpers, Eligio P. Rivero, Modelling of flow distribution within spacer-filled channels fed by dividing manifolds as found in stacks for membrane-based technologies, Chemical Engineering Journal, 423 (2021) 130232, https://doi.org/10.1016/j.cej.2021.130232

[26] Usman Hamid, Cheng-Ju Hsieh, Haoran Wu, Lauren Valentino, Meltem Urgun-Demirtas, and Chau-Chyun Chen, Adsorption Equilibrium, Kinetics, and Column Breakthrough Data of Acetic Acid, Butyric Acid, and Lactic Acid on the IRN-78 Ion-Exchange Resin at Initial pH (∼3−7) and Temperature (25−55 °C), J. Chem. Eng. Data, 69 (2024) 4454−4465, https://doi.org/10.1021/acs.jced.4c00184

[27] A.B. Moldes, J.L. Alonso, J.C. Parajo, Recovery of lactic acid from simultaneous saccharification and fermentation media using anion exchange resins, Bioprocess Biosyst Eng, 25 (2003) 357–363, https://doi:10.1007/s00449-002-0316-7

[28] Isidro J. González-Panzo, Gustavo Aparicio-Mauricio, María Aurora Martínez-Trujillo, Martín R. Cruz-Díaz, Experimental study, modeling and simulation of lactic acid recovery by the electrodeionization cell, Sep. Purif. Technol., 397(3) (2026) 138050, https://doi.org/10.1016/j.seppur.2026.138050

[29] Isidro J. González-Panzo, Martín R. Cruz-Díaz, Eligio P. Rivero, Approach to chemical equilibrium of water dissociation for modeling bipolar membranes in acid-base flow batteries, Electrochimica Acta, 462 (2023) 142755, https://doi.org/10.1016/j.electacta.2023.142755

[30] Georgios Sakas, Alejandro Ibáñez-Rioja, Vesa Ruuskanen, Antti Kosonen, Jero Ahola, Olli Bergmann, Dynamic energy and mass balance model for an industrial alkaline water electrolyzer plant process, International Journal of Hydrogen Energy, 47(7) (2022) 4328-4345, https://doi.org/10.1016/j.ijhydene.2021.11.126

[31] Yoon Koo Lee, *et al.*, A Comprehensive Experimental and Modeling Study on Dissolution in Li-Ion Batteries, J. Electrochem. Soc., 166 (2019) A1340, https://doi.org/10.1149/2.0111908jes

[32] D. Butylskii, V. Troitskiy, D. Chuprynina, L. Dammak, C. Larchet, V. Nikonenko, Application of Hybrid Electrobaromembrane Process for Selective Recovery of Lithium from Cobalt- and Nickel-Containing Leaching Solutions, Membranes, 13 (2023) 509. https://doi.org/10.3390/membranes13050509

[33] K.E. Bouhidel, & A. Lakehal, Influence of voltage and flow rate on electrodeionization (EDI) process efficiency, Desalination, 193 (2006) 411–421, https://doi.org/10.1016/j.desal.2005.08.027

[34] Z. Foo, T.R. Lee, J.M. Wegmueller, S.M. Heath, & J.H. Lienhard, Toward a Circular Lithium Economy with Electrodialysis: Upcycling Spent Battery Leachates with Selective and Bipolar Ion-Exchange Membranes, Environmental Science & Technology, 58 (2024) 19486–19500, https://doi.org/10.1021/acs.est.4c06033

[35] Z. Xing, & M. Srinivasan, Lithium recovery from spent lithium-ion batteries leachate by chelating agents facilitated electrodialysis. Chemical Engineering Journal, 474 (2023) 145306, https://doi.org/10.1016/j.cej.2023.145306

[36] A. M. N. de O. Lima, D. C. R. Espinosa, L.A. Gobo, E.A. Kumoto, A.B. Botelho Junior & J.A.S. Tenório, Study of the behaviour of cations in leaching of NCA lithium-ion batteries by electrodialysis. Environmental Technology, 46(16) (2025) 3024–3035, https://doi.org/10.1080/09593330.2025.2451781

[37] J. Zhu *et al.*, Bipolar membranes electrodialysis of lithium sulfate solutions from hydrometallurgical recycling of spent lithium-ion batteries, Separation and Purification Technology, 354(1) (2025) 128715, https://doi.org/10.1016/j.seppur.2024.128715

[38] M.M. Cerrillo-Gonzalez, *et al.*, Recovery of Li and Co from $LiCoO_2$ via Hydrometallurgical–Electrodialytic Treatment, Applied Sciences, 10 (2020) 2367, https://doi.org/10.3390/app10072367